

# Differentiated cell behavior: a multiscale approach using measure theory

Annachiara Colombi, Marco Scianna\*

*Department of Mathematical Sciences  
Politecnico di Torino  
Corso Duca degli Abruzzi 24, 10129 Torino, Italy*

Andrea Tosin

*Istituto per le Applicazioni del Calcolo "M. Picone"  
Consiglio Nazionale delle Ricerche  
Via dei Taurini 19, 00185 Rome, Italy*

## Abstract

This paper deals with the derivation of an Eulerian model of cell population dynamics out of a Lagrangian description of the underlying physical particle system. By looking at the spatial distribution of cells in terms of time-evolving measures, rather than at individual cell paths, an ensemble representation of cell populations is obtained from the phenomenological behavior of the single cells. In particular, the scale of representation of the system, i.e., microscopic/discrete vs. macroscopic/continuous, can be chosen *a posteriori* according only to the spatial structure given to the measures. Such an approach allows one to represent, within a unified modeling framework, biological systems characterized by the coexistence of different functional subsystems (e.g., cell phenotypes), each of which needs a proper spatial description linked to the specific performed function. In particular, the paper provides computational and analytical insights into a two-population hybrid system, with particular emphasis on the role of some biologically relevant parameters both in the dynamical evolution of the cell aggregate and in selected multiscale stability estimates.

**Keywords:** cell populations, functional subsystems, discrete vs. continuous descriptions, multiscale dynamics

**Mathematics Subject Classification:** 35Q70, 35Q92, 92C17

## 1 Introduction

Living systems are characterized by *collective* dynamics that arise from *individual* behaviors and interactions through *multiscale* interconnected processes. More specifically, the evolution of macroscopic cell aggregates, visible by looking at the totality of cells as a whole, results from the phenomenology of single microscopic cells, that are able to actively sense and interact with the surrounding environment. It appears therefore natural that more and more importance is being paid in Mathematical Biology to the development of multiscale modeling structures capable of ensemble representations while still linking collective dynamics to the small scale cell behaviors (see, for instance, [2, 10, 11, 23] and references therein).

With this broad idea in mind, inspired by the methods developed for crowd dynamics in [8, 9, 20, 21, 25], we here propose a measure-theoretic approach to the modeling of cell populations, which permits a coherent passage from an individual description of single cell behaviors to a

---

\*This author has been funded by a post-doctoral research scholarship awarded by the National Institute for Advanced Mathematics "F. Severi" (INdAM, Italy).

collective representation of the aggregate distribution in terms of time-evolving measures. More specifically, we admit that cell positions are microscopic variables, say  $X_t^i$  ( $i = 1, \dots, N$ , where  $t$  is time and  $N$  is the size of the population), whose evolution in time is determined by hybrid differential equations implementing interactions between *individual* cells and the *collective* distribution of the surrounding mass. Then we resort to some ideas from the transport of measures, in a mass-conservative framework, for abstracting the time evolution of the  $X_t^i$ 's into the spatiotemporal evolution of a measure  $\mu_t$  representing their aggregate Eulerian distribution in space. Mass conservation is here motivated by the fact that, at the individual cell level, we consider only conservative interactions, i.e., interactions which do not change the number of involved particles. Thus, it makes sense to assume that the aforesaid measure is simply moved and redistributed by some velocity field, which has to be properly linked to the microscopic cell behavior and, besides the already mentioned cell interactions, may also include a component determined by an extracellular chemical substance (i.e., via chemotactic or haptotactic mechanisms).

With this procedure, we naturally pass from a Lagrangian to an Eulerian description, while still preserving the finiteness of both the total number of cells (i.e., we do not take the limit  $N \rightarrow \infty$ ) and the individual mass of the latter (which does not become infinitesimal). Therefore all quantities, such as the cell sensing radii and the intercellular interaction strengths, can still be directly referred to the characteristic cell scale. The resulting mathematical structure enables one to derive discrete or continuous models from the very same abstract framework only by acting on the spatial structure of the measure  $\mu_t$  (atomic or absolutely continuous with respect to Lebesgue, respectively). It is worth pointing out that, in our case, the continuous and discrete descriptions should not be understood as a sort of approximation of one another. In fact, as implied above, the “microscopic vs. macroscopic” dichotomy is here not meant in terms of space averages of an infinite number of massless (in the limit) particles. This makes the difference between the proposed approach and classical approaches presented in the literature, which typically rely on the idea that the continuous description emerges in the limit from a vanishing discrete description, and is thus a good approximation of the latter for very large numbers of particles. For instance, in [24], a macroscopic chemotaxis system describing aggregation phenomena due to cell chemical responses to a diffusing substance is derived as the limit of an interacting stochastic many-particle system, where the interaction among the particles is suitably rescaled as the population size tends to infinity. In [6], the authors employ a *mean-field limit* to pass from microscopic/Cucker-Smale-type models of swarming to a statistical representation by means of kinetic equations, still in the limit of an infinite number  $N$  of particles whose mass is scaled as  $1/N$ . In [4, 17], a heuristic *law of large numbers* is instead used to derive a deterministic macroscopic/Eulerian model for the evolution of systems of interacting particles by scaling up from a microscopic/Lagrangian description of individual dynamics, determined by sets of Itô-type stochastic differential equations. This approach is employed by the same authors to study tumor-induced angiogenic processes [5]. Finally, in [13] a cellular automaton model is the starting point to construct a multivariate master equation, from which a continuous model is derived by a systematic *coarse-graining procedure*. This method consists in expressing the rules of the cellular automaton in terms of chemical reactions and in focusing on the evolution of spatial compartments which contain a sufficiently high number of massless cells.

Our approach is of particular relevance in biological systems composed by several functional subsystems, for instance multiple cell populations or multiple clones of the same population, which individually require a distinct type of mathematical description according to their specific functions and behaviors. For instance, few specialized/differentiated cells can be properly described by a concentrated (i.e., discrete) representation. On the other hand, nonspecialized/undifferentiated cells can be represented as a continuously distributed group with low individual detail. Such a discrete-continuous coupling is expected to provide a useful approach for a wide range of biological phenomena. It is, for example, the case of wound healing processes or of blood vessel formation and development, where a small number of activated cells behave as a migratory guidance for the collective patterning of the rest of the aggregate. Typical phenotypic differences are also observed in pathological situations, such as in tumor growth. Nutrient gradients form in fact within a solid cancer mass, causing a well-localized differentiation of malignant cells, which typically

differentiate in an outer viable rim of highly metabolic and proliferative individuals and a central quiescent (possibly necrotic) core. In particular, the external cells, which are difficult to be clinically detected, have the greatest potential to metastasize, displaying an evident ability to evade destruction by the immune system, enter the host bloodstream or lymphatics, extravasate at a distant site, and establish secondary colonies with devastating consequences for the wellbeing of the patient. According to these considerations, a discrete description is biologically appropriate for the cells at the external ring of a tumor, whereas a continuous approximation is natural to represent the inner core of a malignant mass.

After the above general presentation, the contents of the paper can now be outlined more precisely. In Section 2, we introduce the mathematical structures based on time-evolving measures and we derive the Eulerian model for the evolution of cell aggregates out of the Lagrangian description of single cell behavior. In Section 3, we rest on a two-population system, where few activated/discrete cells drive the evolution of an undifferentiated/continuous mass. In Section 4, we perform a computational analysis of our method by means of exploratory case studies which investigate the joint influence of the spatial representation and of some biologically relevant model parameters on the resulting cell dynamics. Finally, in Section 5, we propose an analytical study, whose purpose is to inquire into the similarities and differences in the dynamics of the two-population system caused by choosing *a priori* a discrete or a continuous representation for the population of undifferentiated cells.

## 2 Mathematical model

We consider a biological system formed by  $p$  functional subsystems, viz. cell populations, each of them with a finite and constant number of individuals  $N_i$  (i.e., we are assuming that cells do not undergo mitosis or apoptosis). The evolution of a generic representative cell of population  $i$ , hereafter called *test cell*, is then described at the suitable *individual* scale by means of a variable  $X_{t,i}$ ,  $t \geq 0$ , which takes values in  $\mathbb{R}^n$ . If an initial position  $X_{0,i} = x_0 \in \mathbb{R}^n$  is assigned, the mapping  $t \mapsto X_{t,i}(x_0)$  represents the trajectory of the cell placed in  $x_0$  at the initial time  $t = 0$ , i.e., we are taking a Lagrangian point of view. A practical assumption for reducing the complexity of the problem is that the cells within the same population are *indistinguishable* from one another, in the sense that if initially two cells belonging to the  $i$ -th population switch their positions, the dynamics observed at future times are the same.

The total mass of the cell population  $i$  is instead described by a Radon positive measure  $\mu_{t,i}$ , that we assume to be defined on the Borel  $\sigma$ -algebra  $\mathcal{B}(\mathbb{R}^n)$ . For any measurable set  $E \in \mathcal{B}(\mathbb{R}^n)$ , the value  $\mu_{t,i}(E) \geq 0$  measures the mass of cells located in  $E$  at time  $t \geq 0$ . In particular, the  $\sigma$ -additivity of  $\mu_{t,i}$  directly translates the concept of the additivity of physical masses so that

$$\mu_{t,i}(\mathbb{R}^n) = N_i, \quad \forall t \geq 0. \quad (1)$$

Summarizing,  $X_{t,i}$  is characteristic of an *individual* description, whereas the measure  $\mu_{t,i}$  looks at the system from a *collective* point of view, not necessarily focused on single cells.

### 2.1 Particle models

To approach the dynamics of the test cell, we recall that biological individuals are not passively prone to Newtonian laws of inertia, but are able to actively develop behavioral strategies which depend both on specific internal stimuli and on the interaction with the external environment (other cells, chemical fields or extracellular matrix components). Furthermore, in extremely viscous regimes, such as the biological environments themselves, the velocity of moving individuals and not their acceleration is typically proportional to the sensed forces (*overdamped force-velocity response*, characteristic of several Individual-Based Models [13, 14, 22]).

These concepts, also developed for other systems of living entities, such as human crowds [3], can be translated into mathematical terms by a direct modeling of the velocity of the cells. In particular, we here assume that the dynamics of a cell in an aggregate result from i) a specific

directional movement and ii) its interactions with the ensemble distribution of surrounding individuals. A prototype for the evolution equation of the variable  $X_{t,i}$  then writes as:

$$\dot{X}_{t,i} = v_{\text{chem},i}(t, X_{t,i}) + v_{\text{int},i}(X_{t,i}) = v_{\text{chem},i}(t, X_{t,i}) + \sum_{j=1}^p \int_{\mathbb{R}^n \setminus \{X_{t,i}\}} H_{ij}(y - X_{t,i}) d\mu_{t,j}(y). \quad (2)$$

The term  $v_{\text{chem},i} : \mathbb{R}^n \rightarrow \mathbb{R}^n$  implements a motion field generated either by the topology of the extracellular environment (i.e., via durotactic or haptotactic mechanisms) or by the spatial distribution of some diffusive chemical the test cells are sensitive to (i.e., via chemotaxis).

The term  $v_{\text{int},i}$  represents instead the interaction component of the velocity, which accounts for binary intercellular adhesive/repulsive interactions defined by kernels  $H_{ij} : \mathbb{R}^n \rightarrow \mathbb{R}^n$ , and performed by the test cell  $X_{t,i}$  through a scanning of the *surrounding mass* (i.e., of its *field cells*). At this regard, the right way to interpret the specific subscripts is the following: the generic interaction kernel  $H_{ij}$  defines how the test individual of population  $i$  is *influenced* in its dynamics *by* a field individual belonging to population  $j$ . In particular, we distinguish between *endogenous* (between individuals of the same population, i.e.,  $j = i$ ) and *exogenous* (between individuals of different populations, i.e.,  $j \neq i$ ) contributions. It is finally natural to assume that the result of the intercellular interactions gives an effect along the direction connecting the interacting individuals, depending for instance on their relative position.

## 2.2 Formal derivation via transport of measures

The phenomenological model (2) involves two types of state variables,  $\mu_{t,i}$  and  $X_{t,i}$ , so far correlated at a conceptual but not yet formal level. A formal link can be established via the following argument: the cell mass  $\mu_{t,i}(E)$ , as a material quantity of a fixed number of cells of the  $i$ -population, has to move coherently with the movement of the single individuals. In mathematical terms, this implies that each  $\mu_{t,i}$  is transported by the corresponding  $X_{t,i}$ . Given an initial mass distribution  $\mu_{0,i}$ , at all successive times  $t > 0$  it therefore results:

$$\mu_{t,i} = X_{t,i} \# \mu_{0,i}. \quad (3)$$

Thus, for any Borel set  $E$ , we have that

$$\mu_{t,i}(E) = \mu_{0,i}(E_0), \quad (4)$$

where

$$E_0 = X_{t,i}^{-1}(E) = \{x_0 \in \mathbb{R}^n : X_{t,i}(x_0) \in E\} \quad (5)$$

has to be understood as the set of all possible initial positions from which a test cell has reached  $E$  at time  $t > 0$ .

From (3), it is now possible to formally derive an evolution equation for each mass measure  $\mu_{t,i}$ . First, let us technically regard the mapping  $t \mapsto \mu_{t,i}$  as a curve in the space of distributions, i.e., in the dual space of the Banach space  $C_c^\infty(\mathbb{R}^n)$  containing the infinitely differentiable functions with compact support in  $\mathbb{R}^n$ . Then, after picking a test function  $\psi \in C_c^\infty(\mathbb{R}^n)$ , the time derivative of  $\mu_{t,i}$  can be computed proceeding as in Reynolds' theorem:

$$\begin{aligned} \frac{d}{dt} \langle \mu_{t,i}, \psi \rangle &= \frac{d}{dt} \int_{\mathbb{R}^n} \psi(x) d\mu_{t,i}(x) = \frac{d}{dt} \int_{\mathbb{R}^n} \psi(X_{t,i}) d\mu_{0,i} = \int_{\mathbb{R}^n} \nabla \psi(X_{t,i}) \cdot \dot{X}_{t,i} d\mu_{0,i} = \\ &= \int_{\mathbb{R}^n} \nabla \psi(X_{t,i}) \cdot (v_{\text{chem},i}(t, X_{t,i}) + v_{\text{int},i}(t, X_{t,i})) d\mu_{0,i} = \\ &= \int_{\mathbb{R}^n} \nabla \psi(x) \cdot (v_{\text{chem},i}(t, x) + v_{\text{int},i}(t, x)) d\mu_{t,i}(x), \end{aligned} \quad (6)$$

where  $\langle \cdot, \cdot \rangle$  denotes the duality pairing in  $C_c^\infty(\mathbb{R}^n)$ . After defining the *transport velocity*

$$v_i[\mu_{t,1}, \dots, \mu_{t,p}](t, x) = v_{\text{chem},i}(t, x) + v_{\text{int},i}(t, x) = v_{\text{chem},i}(t, x) + \sum_{j=1}^p \int_{\mathbb{R}^n \setminus \{x\}} H_{ij}(y - x) d\mu_{t,j}(y), \quad (7)$$

Eq. (6) can be finally recognized as the weak form of a conservation law for the cellular mass, leading to the corresponding strong formulation:

$$\frac{\partial \mu_{t,i}}{\partial t} + \nabla \cdot (\mu_{t,i}(v_{\text{chem},i} + v_{\text{int},i}[\mu_{t,1}, \dots, \mu_{t,p}])) = 0. \quad (8)$$

The above-presented approach is expected to provide consistent mathematical tools to address the multiscale issues posed by biological problems. In fact, the description of the system in terms of an abstract measure does not force an *a priori* choice of the scale of representation of each population, which can then be *a posteriori* deferred *only* to the specific structure given to  $\mu_{t,i}$ . For instance, a *macroscopic/continuous* description of a cellular population requires to assume that the mass measure is absolutely continuous with respect to the  $n$ -dimensional Lebesgue measure  $\mathcal{L}^n$  (i.e.,  $\mu_{t,i} \ll \mathcal{L}^n$ ):

$$\mu_{t,i}^c(E) = \int_E \rho_{t,i}(y) dy, \quad \forall E \in \mathcal{B}(\mathbb{R}^n), \quad (9)$$

where  $\rho_{t,i} : \mathbb{R}^n \rightarrow [0, +\infty)$  is the numerical space *density* of the cell population at time  $t$ , whose existence is asserted by the Radon-Nikodym's Theorem. Conversely, a *microscopic/discrete* description of population  $i$ , in which each cell is individually represented, can be achieved by using an atomic mass measure constituted by a sum of Dirac masses centered in each cell position:

$$\mu_{t,i}^d(E) = \sum_{k=1}^{N_i} \delta_{x_{t,i}^k}(E), \quad \forall E \in \mathcal{B}(\mathbb{R}^n), \quad (10)$$

where  $\{x_{t,i}^k\}_{k=1}^{N_i}$  are the space positions where the  $N_i$  cells are located at time  $t$ , i.e.,  $x_{t,i}^k = X_{t,i}(x_{0,i}^k)$ .

The proposed modeling framework differentiates our point of view from other approaches widely studied in the literature, which generally interpret the relationship between discrete and continuous representations in an average sense by means of statistical distributions of mass-vanishing particles (the number of particles is sent to infinity while the total mass of the system is kept finite). Rather, we understand the discrete and continuous scales of description as, in principle, *phenomenologically* different, since, in both cases, the total cellular mass is maintained finite. In other words, we are not describing the continuum as emerging in the limit  $N_i \rightarrow \infty$  from a vanishing discrete representation. Continuous and discrete descriptions are two complementary ways of looking at the same finite-size cell population, which can be associated to complementary phenomenologies exhibited by cells. The model also allows us to use, within the *same* framework, a different level of representation for each population forming the biological system of interest.

### 3 A two population-system

In a wide range of pattern formations, characteristic of biological processes, large aggregates of non-specialized inactivated cells are collectively guided by a small number of specialized and activated individuals (often belonging to the same cell lineage). This is for example what happens in angiogenesis, in morphogenesis, in wound healing mechanisms, or in the metastatic infiltration of solid tumors [15, 16]. On one side, such differentiated cells need to be properly described by a concentrated (i.e., discrete) distribution. On the other, the undifferentiated cell aggregates can be represented, on the whole, as a continuously distributed group with a low individual level of detail.

In order to formalize the mathematical description of such a case, we set up a two-population system, where the first population, whose mass distribution at time  $t$  is denoted by  $\mu_{t,1}^c$ , is composed by a possibly high number of unspecialized cells  $N_1$ , whereas the second one, whose mass distribution at time  $t$  is denoted by  $\mu_{t,2}^d$ , comprises a much lower number of differentiated cells  $N_2 \ll N_1$ . Applying the mathematical structures presented in the previous section, i.e., plugging

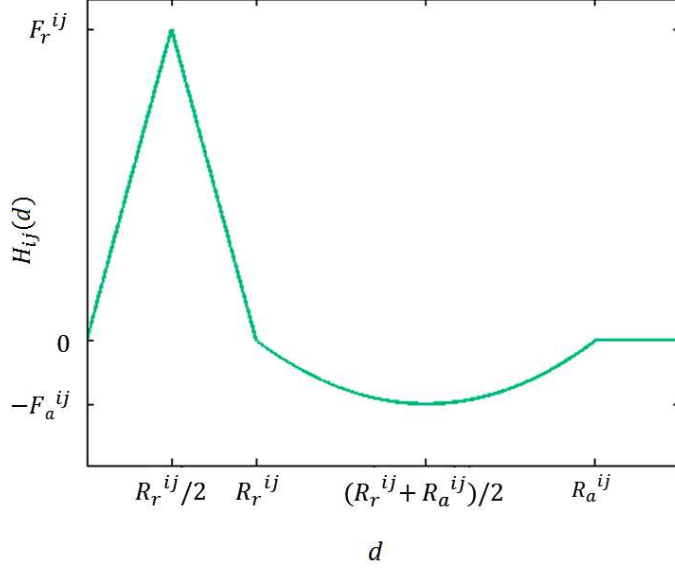


Figure 1: Plot of the proposed interaction kernels  $H_{ij}$  (cf. Eq. (15)).  $R_r^{ij}$  and  $R_a^{ij}$  are the repulsive and the attractive radii, respectively, whereas  $F_r^{ij}$  and  $F_a^{ij}$  are the corresponding strengths.

either (9) or (10) in (6), the evolution of the whole biological environment is determined by the following system of *coupled* discrete-continuous equations, which consists of a conservation equation for the mass density  $\rho_{t,1}$  and of a set of ODEs for the discrete variables  $x_{t,2}^k$ , where  $k = 1, \dots, N_2$ :

$$\begin{cases} \frac{\partial \rho_{t,1}}{\partial t} + \nabla \cdot (\rho_{t,1} v_1[\mu_{t,1}^c, \mu_{t,2}^d]) = 0 \\ \frac{dx_{t,2}^k}{dt} = v_2[\mu_{t,2}^d, \mu_{t,1}^c](x_{t,2}^k) \quad (k = 1, \dots, N_2), \end{cases} \quad (11)$$

where the velocity fields specialize as

$$\begin{cases} v_1[\mu_{t,1}^c, \mu_{t,2}^d](t, x) = \underbrace{\int_{\mathbb{R}^n} H_{11}(y-x) d\rho_{t,1}(y) + \sum_{k=1}^{N_2} H_{12}(x_{t,2}^k - x)}_{v_{\text{int},1}} \\ v_2[\mu_{t,2}^d, \mu_{t,1}^c](x_{t,2}^k) = v_{\text{chem},2}(t, x_{t,2}^k) + \underbrace{\int_{\mathbb{R}^n} H_{21}(y-x_{t,2}^k) d\rho_{t,1}(y) + \sum_{\substack{j=1 \\ j \neq k}}^{N_2} H_{22}(x_{t,2}^j - x_{t,2}^k)}_{v_{\text{int},2}}. \end{cases} \quad (12)$$

It is assumed that a chemotactic component of the velocity is present only for differentiated cells, which are sensitive to chemicals since they typically express surface receptors. In particular,  $v_{\text{chem},2}$  depends on the local gradient of a molecular variable  $c$ , e.g.

$$v_{\text{chem},2}(t, x) = k_0 \nabla c(t, x), \quad (13)$$

where  $k_0$  is a chemotactic strength. The chemical substance instead evolves satisfying a standard reaction-diffusion problem:

$$\begin{cases} \frac{\partial c}{\partial t} = D \Delta c + \alpha - \frac{c}{\tau} & x \in \Omega \subseteq \mathbb{R}^n, t \in (0, T) \\ c = \beta & \text{on } \partial\Omega_1 \\ \frac{\partial c}{\partial n} = 0 & \text{on } \partial\Omega_2, \end{cases} \quad (14)$$

where  $D$  is the constant and homogeneous diffusion coefficient and  $1/\tau$  the decay rate. The secretion rate  $\alpha = \alpha(t, x)$  and the boundary concentration  $\beta = \beta(t, x)$  describe where the chemical substance is produced.

Assuming isotropic adhesive/repulsive interactions, for all  $i, j = 1, 2$ , the kernels  $H_{ij}$  are set to have the following form, see Fig. 1,

$$H_{ij}(d) = \begin{cases} 2\frac{F_r^{ij}}{R_r^{ij}}d & \text{if } 0 \leq |d| < \frac{R_r^{ij}}{2} \\ -2\frac{F_r^{ij}}{R_r^{ij}}d + 2F_r^{ij} & \text{if } \frac{R_r^{ij}}{2} \leq |d| < R_r^{ij} \\ 4F_a^{ij} \frac{(d - R_r^{ij})(d - R_a^{ij})}{(R_r^{ij} - R_a^{ij})^2} & \text{if } R_r^{ij} \leq |d| < R_a^{ij} \\ 0 & \text{if } |d| \geq R_a^{ij}, \end{cases} \quad (15)$$

where  $R_r^{ij}, R_a^{ij} > 0$  are the repulsive and adhesive radii and  $F_r^{ij}, F_a^{ij} > 0$  the corresponding strengths. Notice that, by fixing the interaction radii, we are introducing *metric* intercellular interactions (i.e., within given maximum distances). Furthermore, in the case of two clones of the same cell line (i.e., population 2 is the activated counterpart of population 1), we can consistently take  $R_a^{ij} = R_a$ ,  $R_r^{ij} = R_r$  and  $F_r^{ij} = F_r$  for all  $i, j = 1, 2$ .

## 4 Numerical simulations

In this section, we perform numerical simulations produced by a modified version of the numerical scheme developed in [8] (see also [18, 21] for error and convergence analysis), specifically designed for integrating the evolution of a diffusing substance within the basic measure-theoretic framework.

We deal with a two-dimensional ( $n = 2$ ) square bounded domain  $\Omega \subset \mathbb{R}^n$ , which is set to represent a  $900 \mu\text{m} \times 900 \mu\text{m}$  section of a Petri dish, typically used for *in vitro* biological/biomedical assays. The computational time step  $\Delta t$  is assumed to correspond to approximately 10 seconds: the overall simulations are typically stopped after  $T = 3600\Delta t$ , so that they reproduce a time-lapse of nearly 12 hours.

In all realizations, the initial configuration of the system consists of few differentiated cells belonging to population 2 homogeneously distributed on the edge of a colony of inactivated individuals belonging to population 1. The number  $N_2$  of activated individuals will change in the different sets of simulations, whereas the number of cells within the continuous aggregate is fixed equal to  $N_1 = 100$ . In particular, population 1 is initially arranged into a homogeneous and round colony, so that

$$\rho_{0,1}(x) = \begin{cases} \frac{100}{\pi R_0^2} & \text{if } x \in B_{R_0} \\ 0 & \text{otherwise} \end{cases} \quad (16)$$

where  $B_{R_0} \subset \Omega$  is a ball centered in the middle of the domain and  $R_0 = 100 \mu\text{m}$  is its initial radius. This type of configuration may reproduce a tumor spheroid with an external ring of highly metabolic metastatic cells and an inner core of quiescent individuals, or an endothelial/epithelial cell system where few tip individuals are able to act as guidance leaders for migration for the rest of the stalk/follower mass.

The parameters introduced in the interaction kernels (15), describing the biophysical properties of the cells, can be evaluated consistently with biological considerations. In particular, the common repulsive radius  $R_r$  is fixed equal to  $20 \mu\text{m}$  (that is the average size of most eukaryotic cells) while the attractive one  $R_a$  (that represents the maximal extension of cell filopods) can reach  $60 \mu\text{m}$ . The intercellular repulsive strength  $F_r$  is taken equal to  $1 \mu\text{m} \cdot \text{s}^{-1}$ . Conversely, the magnitude of the adhesive forces will change to reproduce different quantities of expressed cell adhesion molecules (CAMs). The microenvironmental chemical is assumed to be produced only at the boundary of the domain (or in a part of it, see the following sections), and to diffuse and decay within the

entire virtual Petri dish. In particular, referring to Eq. (14), we set  $\alpha = 0$ ,  $\beta = 0.25 \mu\text{M} \cdot \text{s}^{-1}$ ,  $D = 10 \mu\text{m}^2 \cdot \text{s}^{-1}$  and  $\tau = 5000 \text{ s}$ : these are typical values for some important growth factors, such as many isoforms of the Vascular Endothelial Growth Factor (VEGF). Finally, the strength of the chemotactic term of population 2, i.e.,  $k_0$ , will be established in the following.

For a detailed analysis of the role played by the different model parameters, as well as for the corresponding sensitivity analysis, we refer to [7].

## 4.1 Symmetric chemical field

Let us investigate the evolution of the aforesaid cell system in the case of a symmetric chemical field, obtained by assuming that a constant production of the substance occurs on the entire boundary of the domain, i.e.,  $\partial\Omega_1 \equiv \partial\Omega$  and  $\partial\Omega_2 = \emptyset$  in Eq. (14).

In particular, in this first set of simulations we analyze cellular dynamics for different numbers of discrete individuals  $N_2$ . In these cases, the chemotactic strength is  $k_0 = 500 \mu\text{m}^2 \cdot \mu\text{M}^{-1} \cdot \text{s}^{-1}$ , while the matrix collecting the adhesive interaction strengths is set to

$$F_a = \begin{pmatrix} 0.04 & 0.203 \\ 0.0038 & 0.00025 \end{pmatrix} \mu\text{m} \cdot \text{s}^{-1}. \quad (17)$$

The value of  $F_a^{11}$  assures that population 1 reaches a sort of inner equilibrium, i.e., the continuous colony does not undergo a dramatic scatter or an unrealistic collapse (see [7] for a detailed analysis). Moreover, this set of parameters allows for a consistent chemotactic migration of the activated cells, as the heterotypic adhesive forces  $F_a^{12}$  and  $F_a^{21}$  are not high enough to cause their absorption within the continuous mass.

Further, we can preliminarily observe that, given the specific assumptions on its production, the concentration of the chemical has a smoothed square profile in the proximity of the boundary of the domain, while stabilizing in a more round configuration towards the middle. For this reason, the chemotactic gradient is obviously higher along the axes than along the diagonal of the square domain. By analyzing Fig. 2, it is then possible to observe the formation of different types of morphological structures, that extend from the continuous colony beside each differentiated individual, being determined by their initial positions:

- cellular *fingers* emerge and fully develop from the undifferentiated aggregate in correspondence of discrete cells initially placed in the direction of the center of the nearest edge;
- *clumped sprout* grow instead from population 1 behind discrete cells initially placed in correspondence of a diagonal of the domain. This phenomenon results from the fact that such activated individuals sense a chemotactic field substantially lower, and therefore they slowly move from the continuous aggregate, so that continuous fingers have not enough time to completely develop before the end of the observation time;
- *curved*, but fully developed *fingers* emerge from the undifferentiated colony 1 in the case of discrete cells placed in intermediate positions between the direction of a corner of the domain and the direction of the central part of a domain edge. This is due to the fact that, in this case, the activated individuals quickly curve during migration, in order to align with the direction of maximal chemical gradient.

The growth rate of the different morphological phenotypes, i.e., nearly  $30 \mu\text{m} \cdot \text{h}^{-1}$  in the case of fully developed (even curved) fingers and nearly  $15 \mu\text{m} \cdot \text{h}^{-1}$  in the case of clumped sprouts, is determined by the velocity of the corresponding leader cell. It is interesting to observe that these values are within the range of the typical speed measured for most endothelial cell lines (also of malignant origin).

Fixing  $N_2 = 4$ , we now turn to investigating the role played by some relevant model parameters. An increment of two orders of magnitude in the value of  $F_a^{21}$  (i.e.,  $= 0.38 \mu\text{m} \cdot \text{s}^{-1}$ ), which as seen measures the attractive potential exerted *by* the undifferentiated cells *on* the discrete individuals, results in a partial disruption of the fingering process, see Fig. 3 (top-center panel). In fact, only

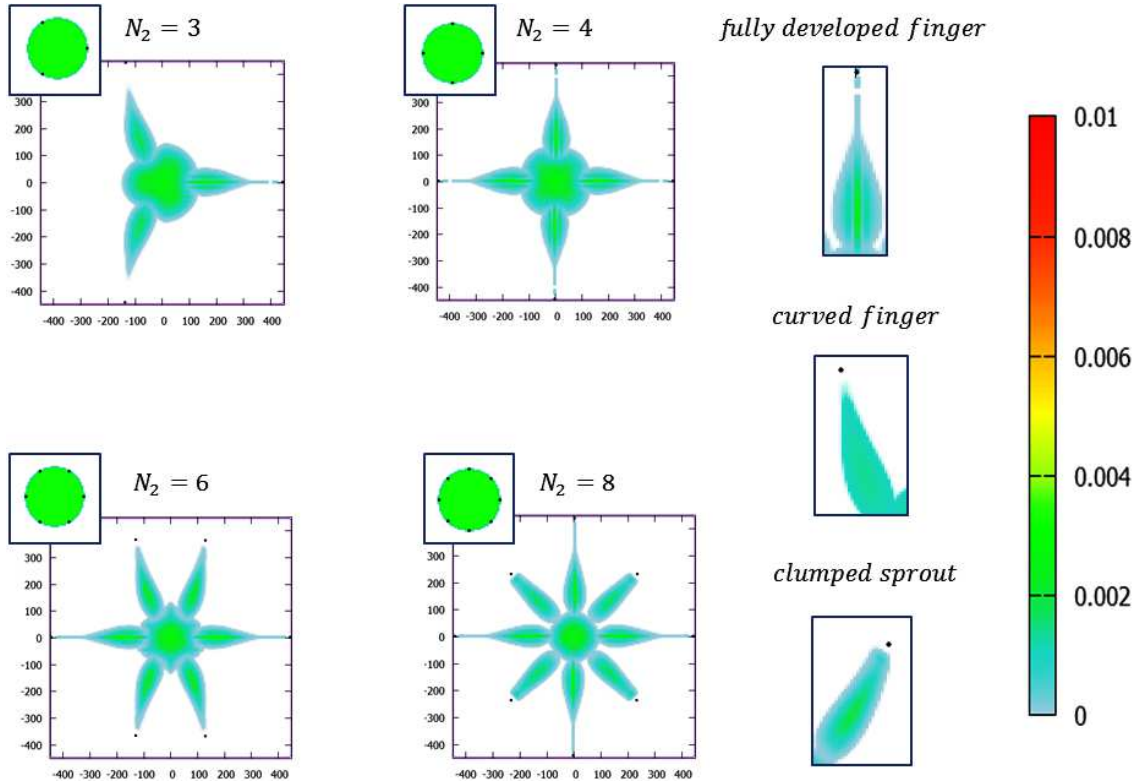


Figure 2: Final configurations (i.e., at  $T = 3600\Delta t \approx 12$  hours) of the two-population system for different numbers of activated cells. As represented in the insets, all initial configurations consist of a round aggregate of undifferentiated individuals surrounded by a homogeneously distributed ring of discrete cells. The parameter setting is described along the text, in particular, the adhesive strengths are summarized in (17).

clumped sprouts emerge, which are characterized by a higher cellular density but a lower growth rate w.r.t. fully developed fingers. This can be explained observing that the chemotactic migration of the activated cells is partially inhibited by the increased intercellular adhesive interactions. Finally, for  $F_a^{21} > 1 \mu\text{m} \cdot \text{s}^{-1}$ , the activated individuals are absorbed within the continuous colony, which undergoes an inner reorganization, possibly stabilizing into a four cluster-morphology (with each cluster containing a discrete cell), as reproduced in the top-right panel of Fig. 3. This phenomenon is due to the fact that the exogenous attractive force is high enough to prevent at all the chemotactic movement of the leader individuals, which are therefore attracted more by the surrounding undifferentiated mass than by the chemical source.

A similar influence on the evolution of the cellular system can be observed in the case of increments in the endogenous adhesive strength of the population 1, see Fig. 3 (middle panels). In fact, at  $F_a^{11} \approx 1 \mu\text{m} \cdot \text{s}^{-1}$ , four thin sprouts detach from the continuous mass and follow the discrete leaders. In particular, such motile structures are characterized by a higher cellular concentration in the trailing edge. The remaining part of population 1 instead undergoes a significant morphological transition towards a cross-like shape. At significantly larger values of  $F_a^{11}$  (i.e.,  $> 1 \mu\text{m} \cdot \text{s}^{-1}$ ), the differentiated cells possibly escape from the continuous spheroid, which remains still and reorganizes into nine small and dense clusters. It is interesting to notice that these little cellular islands are exactly located at the center of the initial colony and, referring to the previous case, at the extremes of the cross-like shape and in the center of the dense trailing part of the emerging sprouts.

We finally vary the chemotactic strength of the discrete cells, see Fig. 3 (bottom panels). A

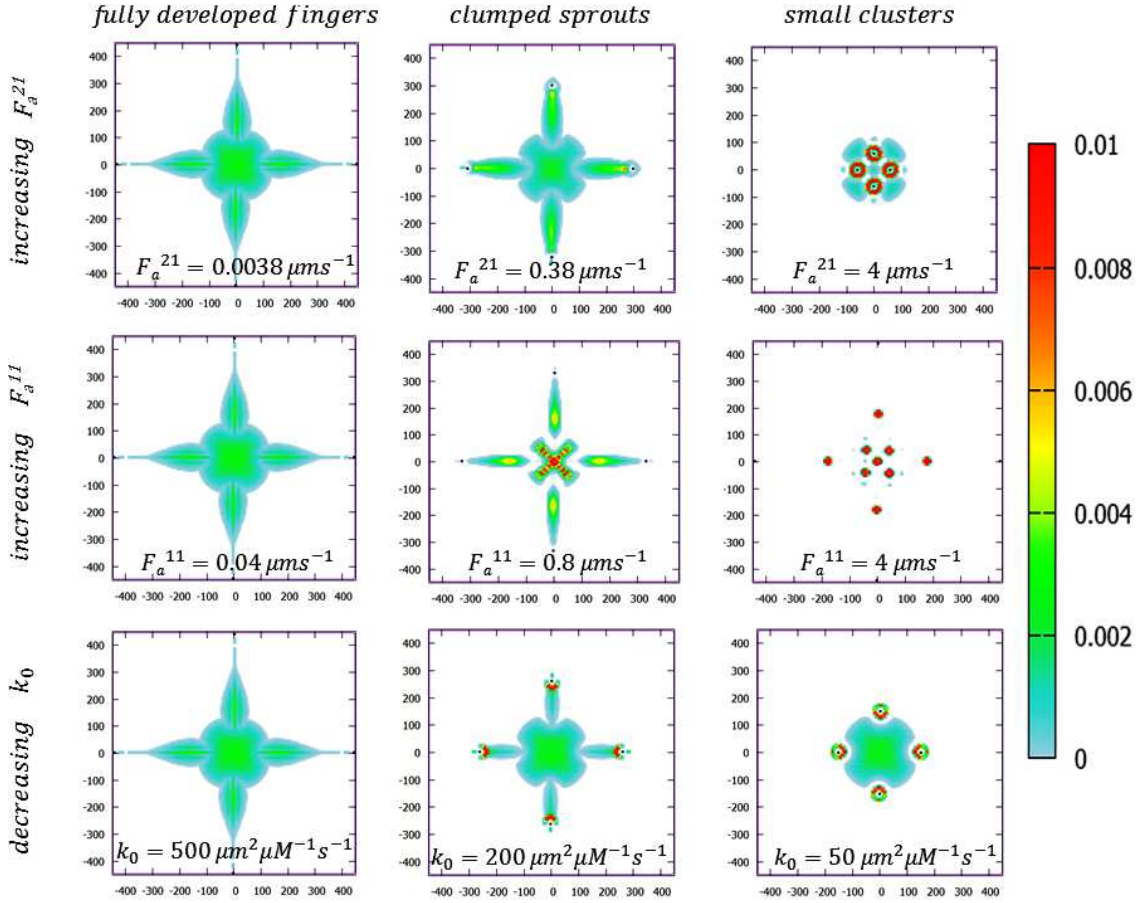


Figure 3: Final configurations (i.e., at  $T = 3600\Delta t \approx 12$  hours) of the two-population system for different values of either the adhesive strengths  $F_a^{21}$  and  $F_a^{11}$ , or the chemotactic sensitivity  $k_0$ . All other parameters, which do not vary with respect to the simulations of Fig. 2, are clarified along the text.

drop of  $k_0$  from  $500 \mu\text{m}^2 \cdot \mu\text{M}^{-1} \cdot \text{s}^{-1}$  to  $200 \mu\text{m}^2 \cdot \mu\text{M}^{-1} \cdot \text{s}^{-1}$  results in a partial inhibition of the fingering process. A decrement of relative importance of the directional velocity for the activated individuals, accompanied by the relative increment of the importance of the exogenous adhesive interactions, leads to the (slow) formation of thin and short sprouts, that are characterized by a higher cellular density in their frontal part, i.e., around the leader cells. At even lower values of  $k_0$  (i.e.,  $\leq 100 \mu\text{m}^2 \cdot \mu\text{M}^{-1} \cdot \text{s}^{-1}$ ), all the discrete individuals are retained within small clusters, stabilized in the proximity of the boundary of the non-motile continuous mass, whose bulk remains, in turn, in a non-motile, quasi-rigid configuration. The chemotactic force is in fact no longer able to overcome the exogenous adhesive interactions.

In summary, we can distinguish three different phenotypes of cell dynamics, each of them characteristic of a specific parameter range: the fingering process, which emerges in the case of low values of both  $F_a^{21}$  and  $F_a^{11}$  and/or of high values of  $k_0$ ; the formation of short and clumped sprouts, obtained by increasing such adhesive strengths and/or by decreasing the chemotactic strength; and, finally, the aggregate clusterization into small islands, characteristic of dramatically high values of  $F_a^{21}$  and  $F_a^{11}$  and/or of low enough values of  $k_0$ .

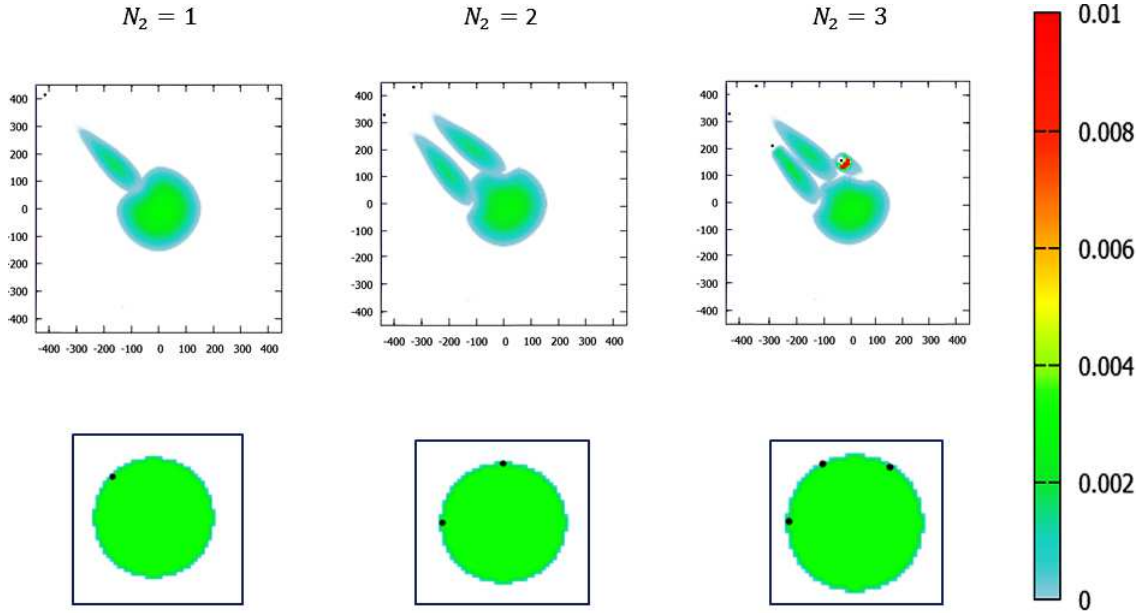


Figure 4: Final configurations (i.e., at  $T = 3600\Delta t \approx 12$  hours) of the two-population system for different numbers and locations of the activated cells, in the case of an asymmetric chemical field obtained by assuming that the chemical production occurs only at the top-left part of the border of the domain. The bottom insets represent the initial configurations of the cellular aggregate. The parameter setting is the same of the simulations presented in Fig. 2.

## 4.2 Asymmetric chemical field

We now turn to study the case of an angular source of chemical field, as the diffusive substance is only produced near the upper-left corner of the domain, i.e.,

$$\partial\Omega_1 = \{(x, y) \in \partial\Omega : x = -450 \mu\text{m}, y \in [400, 450] \mu\text{m} \text{ or } x \in [-450, -400] \mu\text{m}, y = 450 \mu\text{m}\}.$$

All the parameters regulating the evolution of the chemical factor are the same as in the previous sets of simulations. The initial configuration of the continuous aggregate is again a homogenous and round colony of  $N_1 = 100$  individuals, whereas we vary the number and the location of the discrete cells, which however remain distributed around the undifferentiated mass. The adhesive intercellular strengths remain defined as in Eq. (17), whereas the chemotactic sensitivity is taken as  $k_0 = 500 \mu\text{m}^2 \cdot \mu\text{M}^{-1} \cdot \text{s}^{-1}$ .

As reproduced in Fig. 4 (left panels), in the case of a single activated individual, placed in the direction of the angle of the domain, a finger forms and extends from the continuous aggregate. Such a cellular structure grows as quickly as the movement of the discrete individual towards the source of the chemical. Almost the same phenomenon happens when two discrete cells are symmetrically distributed w.r.t. the direction of the chemical source, although the two emerging fingers are a bit curved (see the central panels of Fig. 4).

It is even more interesting the case of three discrete cells symmetrically distributed at the top-left edge of the continuous colony, see Fig. 4 (right panels). In fact, we can observe the simultaneous formation of the three morphological phenotypes encountered in the previous section: a fully developed finger grows in fact behind the “central” activated individual, a shorter sprout follows the discrete cell “on the left”, and a partial clusterization of the undifferentiated aggregate is localized around “the third” discrete cell. These dynamics are not surprising, as each discrete cell senses a distinct chemotactic gradient (we recall that the diffusive substance is produced only at the top-left corner of the boundary of the domain). In more detail, we can compare such different phenomenologies to those obtained with variations of the chemotactic coefficient  $k_0$  in

the case of the symmetric chemical profile (cf. Fig. 3 bottom panels). In particular, the “central” activated individual is subject to the maximum gradient, which corresponds for instance to the maximum value of  $k_0$  in the previous set of simulations. On the opposite, the differentiated cell “on the right” senses the minimum gradient: this is consistent with the case of the minimum chemotactic strength. Finally, the activated cell “on the left” of the colony senses a gradient of an intermediate steepness: therefore only a clumped sprout can emerge, which is exactly the same cellular structure observed in the case of the intermediate value of  $k_0$ .

## 5 Comparison of discrete and continuous descriptions

In this section, we further investigate the discrete and continuous representations introduced in the setup of two interacting cell populations. While it is clear that population 2, composed by few cells, has to be represented as a pointwise (viz. discrete) mass distribution, the question arises whether population 1 needs a continuous or a discrete representation. Both can in principle be appropriate, even if the phenomenology of the problem naturally leads to choose the continuous description. The purpose of this section is to inquire, using analytical methods, into the similarities and differences in the dynamics of the coupled system caused by choosing *a priori* a discrete or a continuous representation of the first population. In particular, we will use  $\mathbb{R}^n$  as the reference domain, since we aim at investigating the qualitative role of some phenomenological parameters of the model, such as the strength of cell-cell interactions and the interaction radii, without technical constraints that would derive from the presence of boundaries. Finally, it is useful to recall that the evolution equation of the chemical field is not coupled with the system of equations regulating cell dynamics.

In [12], a systematic existence and uniqueness theory for the solutions of systems of evolving mass measures is presented. However, the authors deal with velocity fields composed only by potentials (both symmetrizable and non symmetrizable) describing self- and cross-interactions, without accounting chemotactic contributions that may arise from the dynamics of a diffusing substance. Furthermore, the measure theory therein is employed neither to compare a discrete vs. a continuous description of the same physical mass, nor to use different spatial representations for coexisting but functionally distinct particle subsystems.

### 5.1 Formalization of the problem

After the qualitative presentation set forth above, we now introduce the formulation of the problem and quickly review the tools which we need to study it.

We denote by  $\mathcal{M}_1^N(\mathbb{R}^n)$  the space of positive measures on  $\mathbb{R}^n$  having finite mass  $N$  and finite first moment:

$$\mathcal{M}_1^N(\mathbb{R}^n) := \left\{ \lambda \text{ positive measure on } \mathcal{B}(\mathbb{R}^n) : \lambda(\mathbb{R}^n) = N, \int_{\mathbb{R}^n} |x| d\lambda(x) < +\infty \right\}.$$

The space  $\mathcal{M}_1^N(\mathbb{R}^n)$  is equipped with the (*first*) *Wasserstein metric*

$$W_1(\lambda', \lambda'') := \sup_{\varphi \in \text{Lip}_1(\mathbb{R}^n)} \int_{\mathbb{R}^n} \varphi(x) d(\lambda'' - \lambda')(x), \quad \lambda', \lambda'' \in \mathcal{M}_1^N(\mathbb{R}^n),$$

where  $\text{Lip}_1(\mathbb{R}^n)$  denotes the space of Lipschitz continuous functions  $\varphi : \mathbb{R}^n \rightarrow \mathbb{R}$  with at most unit Lipschitz constant. Usually  $W_1$  is introduced in the context of probability measures, i.e., for measuring distances between measures with unit mass. However, its use for measures with arbitrary mass according to the previous definition is straightforward.

Moreover, we define the space:

$$\mathfrak{M} := \mathcal{M}_1^{N_1}(\mathbb{R}^n) \times \mathcal{M}_1^{N_2}(\mathbb{R}^n)$$

of pairs of positive measures with masses  $N_1, N_2$ , respectively, and finite first moments.  $\mathfrak{M}$  is endowed with the metric

$$\mathcal{W}_1((\lambda'_1, \lambda'_2), (\lambda''_1, \lambda''_2)) := W_1(\lambda'_1, \lambda''_1) + W_1(\lambda'_2, \lambda''_2)$$

for  $(\lambda'_1, \lambda'_2), (\lambda''_1, \lambda''_2) \in \mathfrak{M}$ .

We finally introduce the space  $C([0, T]; \mathfrak{M})$ ,  $T > 0$  being a final time, of curves of measures in  $\mathfrak{M}$  parameterized by time,  $t \mapsto (\lambda_{t,1}, \lambda_{t,2}) \in \mathfrak{M}$ , endowed with the metric

$$\text{dist}((\lambda'_{\bullet,1}, \lambda'_{\bullet,2}), (\lambda''_{\bullet,1}, \lambda''_{\bullet,2})) := \sup_{t \in [0, T]} \mathcal{W}_1((\lambda'_{t,1}, \lambda'_{t,2}), (\lambda''_{t,1}, \lambda''_{t,2})),$$

see also [19, 25].

Like in the previous sections, we denote respectively by  $\mu_{t,1}^d, \mu_{t,1}^c$  the discrete and continuous descriptions of the mass of the first population. The corresponding evolution of the second population, which is always taken as discrete, is then denoted by  $\mu_{t,2}^d, \mu_{t,2}^c$ , respectively. In practice, system (11) can be complemented with either initial condition  $(\mu_{0,1}^d, \mu_{0,2})$ ,  $(\mu_{0,1}^c, \mu_{0,2}) \in \mathfrak{M}$ , which generates either solution  $(\mu_{\bullet,1}^d, \mu_{\bullet,2}^d)$ ,  $(\mu_{\bullet,1}^c, \mu_{\bullet,2}^c) \in C([0, T]; \mathfrak{M})$ . Notice that the initial condition for the second population is the same in both cases. The goal is to study how much similar or different the two solutions are for  $t > 0$  depending on the similarity or the difference of the initial mass distributions  $\mu_{0,1}^d, \mu_{0,1}^c$ . In other words, the main result we are going to establish in the sequel is that for system (11), under suitable assumptions specified below, an *a priori* stability estimate of the form

$$\sup_{t \in (0, T]} \mathcal{W}_1((\mu_{t,1}^d, \mu_{t,2}^d), (\mu_{t,1}^c, \mu_{t,2}^c)) \leq \mathcal{C} W_1(\mu_{0,1}^d, \mu_{0,1}^c) \quad (18)$$

holds,  $\mathcal{C} > 0$  being a constant depending on the parameters of the model. Such an estimate will allow us to compare the hybrid continuous-discrete solution  $(\mu_{t,1}^c, \mu_{t,2}^c)$  with the conceivable fully discrete one  $(\mu_{t,1}^d, \mu_{t,2}^d)$ . More precisely, we will see that, in general, the two solutions do not approach each other when the number  $N_1$  of cells of the first population increases but the similarity between the hybrid continuous-discrete and the fully discrete dynamics is established by some other model parameters.

## 5.2 Preliminaries on the regularity of the velocity field

Estimate (18) essentially relies on the regularity of the transport velocity fields  $v_1, v_2$  appearing in the mass conservation equations of system (11). First, it is not difficult to see that the chemotactic part is Lipschitz continuous in the sense that there exists a constant  $\text{Lip}(v_{\text{chem},2}) > 0$  such that:

$$|v_{\text{chem},2}(t, x_2) - v_{\text{chem},2}(t, x_1)| \leq \text{Lip}(v_{\text{chem},2}) |x_2 - x_1| \quad (19)$$

for all  $x_1, x_2 \in \mathbb{R}^n$  and  $t \in (0, T]$ . In fact, if we assume that the secretion rate  $\alpha = \alpha(t, x)$  in (13) is continuous in time and piecewise continuous in space (including, in particular, the possibility that secretion occurs in specific regions of the domain and vanishes elsewhere), we obtain that the chemical field solving the reaction-diffusion equation is continuous in time and differentiable in space and that the chemical gradient appearing in the definition of velocity the  $v_2$  (see (12)<sub>2</sub>) is continuous in time and in space (actually piecewise-differentiable in space). From these considerations, it follows the regularity of  $\nabla c$ . Notice that we do not need to take into account boundary conditions since we work with  $\mathbb{R}^n$  as the reference domain.

Concerning the interaction part of the velocity  $v_{\text{int},i}[\mu_1, \mu_2]$ , for  $i = 1, 2$ , under the assumption

of Lipschitz continuous kernels  $H_{ij}$ , we have, for all  $(\mu'_1, \mu'_2), (\mu''_1, \mu''_2) \in \mathfrak{M}$  and all fixed  $x \in \mathbb{R}^n$ ,

$$\begin{aligned}
|v_{\text{int},i}[\mu''_1, \mu''_2](x) - v_{\text{int},i}[\mu'_1, \mu'_2](x)| &\leq \left| \int_{\mathbb{R}^n} H_{i1}(y-x) d(\mu''_1 - \mu'_1)(y) \right| \\
&\quad + \left| \int_{\mathbb{R}^n} H_{i2}(y-x) d(\mu''_2 - \mu'_2)(y) \right| \\
&\leq \text{Lip}(H_{i1}) \left| \int_{\mathbb{R}^n} \frac{H_{i1}(y-x)}{\text{Lip}(H_{i1})} d(\mu''_1 - \mu'_1)(y) \right| \\
&\quad + \text{Lip}(H_{i2}) \left| \int_{\mathbb{R}^n} \frac{H_{i2}(y-x)}{\text{Lip}(H_{i2})} d(\mu''_2 - \mu'_2)(y) \right| \\
&\leq \text{Lip}(H_{i1}) W_1(\mu'_1, \mu''_1) + \text{Lip}(H_{i2}) W_1(\mu'_2, \mu''_2) \\
&\leq \max\{\text{Lip}(H_{i1}), \text{Lip}(H_{i2})\} \mathcal{W}_1((\mu'_1, \mu'_2), (\mu''_1, \mu''_2)). \quad (20)
\end{aligned}$$

On the other hand, if  $(\mu_1, \mu_2) \in \mathfrak{M}$  is fixed, for all  $x_1, x_2 \in \mathbb{R}^n$  it results:

$$\begin{aligned}
|v_{\text{int},i}[\mu_1, \mu_2](x_2) - v_{\text{int},i}[\mu_1, \mu_2](x_1)| &\leq \int_{\mathbb{R}^n} |H_{i1}(y-x_2) - H_{i1}(y-x_1)| d\mu_1(y) \\
&\quad + \int_{\mathbb{R}^n} |H_{i2}(y-x_2) - H_{i2}(y-x_1)| d\mu_2(y) \\
&\leq (N_1 \text{Lip}(H_{i1}) + N_2 \text{Lip}(H_{i2})) |x_2 - x_1|. \quad (21)
\end{aligned}$$

Collecting (19)–(21) we can state finally:

**Lemma 5.1** (Regularity of the velocity fields). *For Lipschitz continuous interaction kernels  $H_{ij} : \mathbb{R}^n \rightarrow \mathbb{R}^n$  the transport velocity  $v_i$ ,  $i = 1, 2$ , is Lipschitz continuous as well in  $\mathbb{R}^n \times \mathfrak{M}$ . That is, there exists a constant  $\text{Lip}(v_i) > 0$  such that:*

$$|v_i[\mu''_1, \mu''_2](t, x_2) - v_i[\mu'_1, \mu'_2](t, x_1)| \leq \text{Lip}(v_i) \left( |x_2 - x_1| + \mathcal{W}_1((\mu'_1, \mu'_2), (\mu''_1, \mu''_2)) \right)$$

for all  $x_1, x_2 \in \mathbb{R}^n$ ,  $(\mu'_1, \mu'_2), (\mu''_1, \mu''_2) \in \mathfrak{M}$  and  $t \in (0, T]$ .

In addition, the following estimate for  $\text{Lip}(v_i)$  holds:

$$\text{Lip}(v_i) \leq \text{Lip}(v_{\text{chem},i}) + N_1 \text{Lip}(H_{i1}) + N_2 \text{Lip}(H_{i2}).$$

We recall that in the two population setting previously considered we have  $v_{\text{chem},1} \equiv 0$ .

### 5.3 Notion of solution and trajectories

A pair  $(\mu_{\bullet,1}, \mu_{\bullet,2}) \in C([0, T]; \mathfrak{M})$  is a weak solution to the non-autonomous system (11), if it satisfies

$$\begin{cases} \int_{\mathbb{R}^n} \varphi d\mu_{t,1} = \int_{\mathbb{R}^n} \varphi d\mu_{0,1} + \int_0^t \int_{\mathbb{R}^n} \nabla \varphi \cdot v_1[\mu_{s,1}, \mu_{s,2}] d\mu_{s,1} ds \\ \int_{\mathbb{R}^n} \varphi d\mu_{t,2} = \int_{\mathbb{R}^n} \varphi d\mu_{0,2} + \int_0^t \int_{\mathbb{R}^n} \nabla \varphi \cdot v_2[\mu_{s,2}, \mu_{s,1}] d\mu_{s,2} ds, \end{cases} \quad (22)$$

for all  $\varphi \in C_c^\infty(\mathbb{R}^n)$  and all  $t \in [0, T]$ . Moreover, we can formally check that

$$(\mu_{t,1}, \mu_{t,1}) = (\gamma_t \# \mu_{0,1}, \beta_t \# \mu_{0,1}), \quad t \in (0, T] \quad (23)$$

is a representation formula of the solution if the flows maps  $\gamma_{\bullet}^{(\mu_{\bullet,1}, \mu_{\bullet,2})} : [0, T] \times \mathbb{R}^n \rightarrow \mathbb{R}^n$  and  $\beta_{\bullet}^{(\mu_{\bullet,1}, \mu_{\bullet,2})} : [0, T] \times \mathbb{R}^n \rightarrow \mathbb{R}^n$  satisfy:

$$\begin{cases} \frac{\partial \gamma_t^{(\mu_{t,1}, \mu_{t,2})}}{\partial t} = v_1[\gamma_t^{(\mu_{t,1}, \mu_{t,2})} \# \mu_{0,1}, \beta_t^{(\mu_{t,1}, \mu_{t,2})} \# \mu_{0,2}](t, \gamma_t^{(\mu_{t,1}, \mu_{t,2})}(x)) & x \in \Omega \subseteq \mathbb{R}^n, t \in (0, T] \\ \frac{\partial \beta_t^{(\mu_{t,1}, \mu_{t,2})}}{\partial t} = v_2[\beta_t^{(\mu_{t,1}, \mu_{t,2})} \# \mu_{0,2}, \gamma_t^{(\mu_{t,1}, \mu_{t,2})} \# \mu_{0,1}](t, \beta_t^{(\mu_{t,1}, \mu_{t,2})}(x)) & x \in \Omega \subseteq \mathbb{R}^n, t \in (0, T] \\ \gamma_0(x) = \beta_0(x) = x & x \in \Omega \subseteq \mathbb{R}^n \end{cases} \quad (24)$$

Existence and uniqueness of the above-introduced flow maps, and the fact that they are representation formulas of the solutions of (22), follow from the theory developed in [1]. In particular,  $v_1$  and  $v_2$  satisfy the required assumptions, being both Borel vector fields with global bounds.

Taking into account the Lipschitz continuity of  $v_i$  for  $i = 1, 2$ , we can prove the Lipschitz continuity of the flow maps (24).

**Lemma 5.2.** (i) *Let  $(\mu_{\bullet,1}, \mu_{\bullet,2}) \in C([0, T]; \mathfrak{M})$ , then the flow maps defined by (24) satisfy:*

$$\begin{cases} \left| \gamma_t^{(\mu_{t,1}, \mu_{t,2})}(x_2) - \gamma_t^{(\mu_{t,1}, \mu_{t,2})}(x_1) \right| \leq (1 + \text{Lip}(v_1)t)e^{\text{Lip}(v_1)t} |x_2 - x_1| \\ \left| \beta_t^{(\mu_{t,1}, \mu_{t,2})}(x_2) - \beta_t^{(\mu_{t,1}, \mu_{t,2})}(x_1) \right| \leq (1 + \text{Lip}(v_2)t)e^{\text{Lip}(v_2)t} |x_2 - x_1| \end{cases} \quad (25)$$

for all  $x_1, x_2 \in \mathbb{R}^n$ .

(ii) *Let  $x \in \mathbb{R}^n$ , then*

$$\begin{cases} \left| \gamma_t^{(\mu''_{t,1}, \mu''_{t,2})}(x) - \gamma_t^{(\mu'_{t,1}, \mu'_{t,2})}(x) \right| \leq \text{Lip}(v_1)e^{\text{Lip}(v_1)t} \int_0^t \mathcal{W}_1((\mu''_{s,1}, \mu''_{s,2}), (\mu'_{s,1}, \mu'_{s,2})) ds \\ \left| \beta_t^{(\mu''_{t,1}, \mu''_{t,2})}(x) - \beta_t^{(\mu'_{t,1}, \mu'_{t,2})}(x) \right| \leq \text{Lip}(v_2)e^{\text{Lip}(v_2)t} \int_0^t \mathcal{W}_1((\mu''_{s,1}, \mu''_{s,2}), (\mu'_{s,1}, \mu'_{s,2})) ds. \end{cases} \quad (26)$$

for all  $(\mu'_{\bullet,1}, \mu'_{\bullet,2}), (\mu''_{\bullet,1}, \mu''_{\bullet,2}) \in C([0, T]; \mathfrak{M})$ .

*Proof.* From (24) it follows  $\gamma_t^{(\mu_{t,1}, \mu_{t,2})}(x) = x + \int_0^t v_1[\mu_{s,1}, \mu_{s,2}](s, \gamma_s^{(\mu_{s,1}, \mu_{s,2})}(x)) ds$ , hence:

(i)

$$\begin{aligned} & \left| \gamma_t^{(\mu_{t,1}, \mu_{t,2})}(x_2) - \gamma_t^{(\mu_{t,1}, \mu_{t,2})}(x_1) \right| \\ & \leq |x_2 - x_1| + \int_0^t \left| v_1[\mu_{s,1}, \mu_{s,2}](s, \gamma_s^{(\mu_{s,1}, \mu_{s,2})}(x_2)) - v_1[\mu_{s,1}, \mu_{s,2}](s, \gamma_s^{(\mu_{s,1}, \mu_{s,2})}(x_1)) \right| ds \\ & \leq |x_2 - x_1| + \text{Lip}(v_1) \int_0^t \left| \gamma_s^{(\mu_{s,1}, \mu_{s,2})}(x_2) - \gamma_s^{(\mu_{s,1}, \mu_{s,2})}(x_1) \right| ds, \end{aligned}$$

whence invoking Gronwall's inequality yields

$$\left| \gamma_t^{(\mu_{t,1}, \mu_{t,2})}(x_2) - \gamma_t^{(\mu_{t,1}, \mu_{t,2})}(x_1) \right| \leq (1 + \text{Lip}(v_1)t)e^{\text{Lip}(v_1)t} |x_2 - x_1|$$

and the thesis then follows by bounding  $t$  from above at the right-hand side by  $T$ . The same procedure holds for the flow map of the second population.

(ii)

$$\begin{aligned} & \gamma_t^{(\mu''_{t,1}, \mu''_{t,2})}(x) - \gamma_t^{(\mu'_{t,1}, \mu'_{t,2})}(x) \\ & = \int_0^t \left[ v_1[\mu''_{s,1}, \mu''_{s,2}](s, \gamma_s^{(\mu''_{s,1}, \mu''_{s,2})}(x)) - v_1[\mu'_{s,1}, \mu'_{s,2}](s, \gamma_s^{(\mu'_{s,1}, \mu'_{s,2})}(x)) \right] ds \\ & + \int_0^t \left[ v_1[\mu'_{s,1}, \mu'_{s,2}](s, \gamma_s^{(\mu''_{s,1}, \mu''_{s,2})}(x)) - v_1[\mu'_{s,1}, \mu'_{s,2}](s, \gamma_s^{(\mu'_{s,1}, \mu'_{s,2})}(x)) \right] ds, \end{aligned}$$

therefore we have

$$\begin{aligned} & \left| \gamma_t^{(\mu''_{s,1}, \mu''_{s,2})}(x) - \gamma_t^{(\mu'_{s,1}, \mu'_{s,2})}(x) \right| \\ & \leq \text{Lip}(v_1) \left( \int_0^t \mathcal{W}_1((\mu''_{s,1}, \mu''_{s,2}), (\mu'_{s,1}, \mu'_{s,2})) ds + \int_0^t \left| \gamma_s^{(\mu''_{s,1}, \mu''_{s,2})}(x) - \gamma_s^{(\mu'_{s,1}, \mu'_{s,2})}(x) \right| ds \right), \end{aligned}$$

after taking into account Lemma 5.1. Finally, applying again the Gronwall's inequality we obtain

$$\left| \gamma_t^{(\mu''_{s,1}, \mu''_{s,2})}(x) - \gamma_t^{(\mu'_{s,1}, \mu'_{s,2})}(x) \right| \leq \text{Lip}(v_1) e^{\text{Lip}(v_1)t} \int_0^t \mathcal{W}_1((\mu''_{s,1}, \mu''_{s,2}), (\mu'_{s,1}, \mu'_{s,2})) ds.$$

Again, the same procedure can be applied to the other flow map.  $\square$

## 5.4 Main analytical results

Owing to Lemma 5.2, we are now in a position to prove the main result of this part, which establishes that the discrepancy between the hybrid solution of our two-population system (11) and its fully discrete counterpart is *a priori* controlled by the discrepancy between the continuous and the discrete versions of the initial condition of the population 1.

**Theorem 5.1.** *Let  $(\mu_{\bullet,1}^d, \mu_{\bullet,2}^d), (\mu_{\bullet,1}^c, \mu_{\bullet,2}^c) \in C([0, T]; \mathfrak{M})$  be two solutions of the system (11), corresponding to the initial data  $(\mu_{0,1}^d, \mu_{0,2}^d), (\mu_{0,1}^c, \mu_{0,2}^c) \in \mathfrak{M}$ , respectively (we recall that the discrete population 2 has the same initial condition in both cases). Under the assumption of Lipschitz continuity of the interaction kernels  $H_{ij}$ , for all  $i, j = 1, 2$ , we have the following estimate:*

$$\sup_{t \in [0, T]} \mathcal{W}_1((\mu_{t,1}^d, \mu_{t,2}^d), (\mu_{t,1}^c, \mu_{t,2}^c)) \leq \mathcal{C} \mathcal{W}_1(\mu_{0,1}^d, \mu_{0,1}^c), \quad (27)$$

where  $\mathcal{C} > 0$  is a constant independent of  $\mu_{0,1}^d, \mu_{0,1}^c$ .

*Proof.* Let  $\varphi \in \text{Lip}_1(\mathbb{R}^n)$ , then

$$\begin{aligned} & \int_{\mathbb{R}^n} \varphi d(\mu_{t,1}^c - \mu_{t,1}^d) + \int_{\mathbb{R}^n} \varphi d(\mu_{t,2}^c - \mu_{t,2}^d) \\ & = \int_{\mathbb{R}^n} \varphi(\gamma_t^{(\mu_{t,1}^c, \mu_{t,2}^c)}) d\mu_{0,1}^c - \int_{\mathbb{R}^n} \varphi(\gamma_t^{(\mu_{t,1}^d, \mu_{t,2}^d)}) d\mu_{0,1}^d \\ & \quad + \int_{\mathbb{R}^n} \varphi(\beta_t^{(\mu_{t,1}^c, \mu_{t,2}^c)}) d\mu_{0,2} - \int_{\mathbb{R}^n} \varphi(\beta_t^{(\mu_{t,1}^d, \mu_{t,2}^d)}) d\mu_{0,2} \\ & = \int_{\mathbb{R}^n} \left[ \varphi(\gamma_t^{(\mu_{t,1}^c, \mu_{t,2}^c)}) - \varphi(\gamma_t^{(\mu_{t,1}^d, \mu_{t,2}^d)}) \right] d\mu_{0,1}^c + \int_{\mathbb{R}^n} \varphi(\gamma_t^{(\mu_{t,1}^d, \mu_{t,2}^d)}) d(\mu_{0,1}^c - \mu_{0,1}^d) \\ & \quad + \int_{\mathbb{R}^n} \left[ \varphi(\beta_t^{(\mu_{t,1}^c, \mu_{t,2}^c)}) - \varphi(\beta_t^{(\mu_{t,1}^d, \mu_{t,2}^d)}) \right] d\mu_{0,2} + \underbrace{\int_{\mathbb{R}^n} \varphi(\beta_t^{(\mu_{t,1}^d, \mu_{t,2}^d)}) d(\mu_{0,2} - \mu_{0,2})}_{=0}. \quad (28) \end{aligned}$$

Using the Lipschitz continuity of  $\varphi$  and Lemma 5.2, we have that

$$\begin{aligned} & \left| \varphi(\gamma_t^{(\mu_{t,1}^c, \mu_{t,2}^c)}) - \varphi(\gamma_t^{(\mu_{t,1}^d, \mu_{t,2}^d)}) \right| \leq \left| \gamma_t^{(\mu_{t,1}^c, \mu_{t,2}^c)} - \gamma_t^{(\mu_{t,1}^d, \mu_{t,2}^d)} \right| \\ & \leq \text{Lip}(v_1) e^{\text{Lip}(v_1)t} \int_0^t \mathcal{W}_1((\mu_{s,1}^c, \mu_{s,2}^c), (\mu_{s,1}^d, \mu_{s,2}^d)) ds \quad (29) \end{aligned}$$

and analogously

$$\begin{aligned} \left| \varphi(\beta_t^{(\mu_{t,1}^c, \mu_{t,2}^c)}) - \varphi(\beta_t^{(\mu_{t,1}^d, \mu_{t,2}^d)}) \right| &\leq \left| \beta_t^{(\mu_{t,1}^c, \mu_{t,2}^c)} - \beta_t^{(\mu_{t,1}^d, \mu_{t,2}^d)} \right| \\ &\leq \text{Lip}(v_2) e^{\text{Lip}(v_2)t} \int_0^t \mathcal{W}_1((\mu_{s,1}^c, \mu_{s,2}^c), (\mu_{s,1}^d, \mu_{s,2}^d)) ds. \end{aligned} \quad (30)$$

Then, considering that  $\mu_{0,1}^c(\mathbb{R}^n) = N_1$  and  $\mu_{0,2}(\mathbb{R}^n) = N_2$ :

$$\begin{aligned} \left| \int_{\mathbb{R}^n} \left[ \varphi(\gamma_t^{(\mu_{t,1}^c, \mu_{t,2}^c)}) - \varphi(\gamma_t^{(\mu_{t,1}^d, \mu_{t,2}^d)}) \right] d\mu_{0,1}^c \right| \\ \leq N_1 \text{Lip}(v_1) e^{\text{Lip}(v_1)t} \int_0^t \mathcal{W}_1((\mu_{s,1}^c, \mu_{s,2}^c), (\mu_{s,1}^d, \mu_{s,2}^d)) ds \end{aligned} \quad (31)$$

and

$$\begin{aligned} \left| \int_{\mathbb{R}^n} \left[ \varphi(\beta_t^{(\mu_{t,1}^c, \mu_{t,2}^c)}) - \varphi(\beta_t^{(\mu_{t,1}^d, \mu_{t,2}^d)}) \right] d\mu_{0,2} \right| \\ \leq N_2 \text{Lip}(v_2) e^{\text{Lip}(v_2)t} \int_0^t \mathcal{W}_1((\mu_{s,1}^c, \mu_{s,2}^c), (\mu_{s,1}^d, \mu_{s,2}^d)) ds. \end{aligned} \quad (32)$$

Recalling again the Lipschitz continuity of both  $\varphi$  and  $\gamma_t, \beta_t$  in  $x$  (and therefore of  $\varphi \circ \gamma_t$  and  $\varphi \circ \beta_t$ ), together with Lemma 5.2, the second term at the right-hand side of (28) can be bounded as

$$\left| \int_{\mathbb{R}^n} \varphi(\gamma_t^{(\mu_{t,1}^d, \mu_{t,2}^d)}) d(\mu_{0,1}^c - \mu_{0,1}^d) \right| \leq \left(1 + \text{Lip}(v_1)t e^{\text{Lip}(v_1)t}\right) \mathcal{W}_1(\mu_{0,1}^c, \mu_{0,1}^d). \quad (33)$$

Next, owing to inequalities (29)–(33), adding the analogous terms, and taking the supremum over  $\varphi \in \text{Lip}_1(\mathbb{R}^n)$  of both sides of (28), we get:

$$\begin{aligned} &\mathcal{W}_1((\mu_{t,1}^d, \mu_{t,2}^d), (\mu_{t,1}^c, \mu_{t,2}^c)) \\ &\leq \underbrace{(N_1 \text{Lip}(v_1) e^{\text{Lip}(v_1)t} + N_2 \text{Lip}(v_2) e^{\text{Lip}(v_2)t})}_{\mathcal{C}_1} \int_0^t \mathcal{W}_1((\mu_{s,1}^d, \mu_{s,2}^d), (\mu_{s,1}^c, \mu_{s,2}^c)) ds \\ &\quad + \underbrace{\left(1 + \text{Lip}(v_1)t e^{\text{Lip}(v_1)t}\right)}_{\mathcal{C}_2} \mathcal{W}_1(\mu_{0,1}^c, \mu_{0,1}^d). \end{aligned} \quad (34)$$

Finally, by applying Gronwall's inequality, we obtain the thesis (27) with  $\mathcal{C} := \mathcal{C}_2 e^{\mathcal{C}_1 T}$ .  $\square$

The Lipschitz constants determining  $\mathcal{C}$  in (27) can be specified taking into account the estimates established in Lemma 5.1 for  $\text{Lip}(v_i)$ , with  $i = 1, 2$ :

$$\begin{cases} \text{Lip}(v_1) = 2N_1 \max \left\{ \frac{F_r}{R_r}; \frac{F_a^{11}}{R_r} \right\} + 2N_2 \max \left\{ \frac{F_r}{R_r}; \frac{F_a^{12}}{R_r} \right\}, \\ \text{Lip}(v_2) = k_0 \text{Lip}(\nabla c) + 2N_1 \max \left\{ \frac{F_r}{R_r}; \frac{F_a^{21}}{R_r} \right\} + 2N_2 \max \left\{ \frac{F_r}{R_r}; 2 \frac{F_a^{22}}{R_r} \right\}, \end{cases}$$

where the specific form of the interaction kernels given in (15), as well as the biological considerations mentioned at the end of Section 3 on the values taken by the repulsive radii and by the corresponding repulsive strengths in the case of the proposed two-population system, are considered. We can therefore state that, in principle, decrements in the strength of the intercellular interactions (both repulsive and attractive) or increments in the corresponding radii have a stabilizing effect on the evolution of the discrepancy between the hybrid and the fully discrete solutions of system (11).

## References

- [1] L. Ambrosio, N. Gigli, and G. Savaré. *Gradient Flows: In Metric Spaces And In The Space Of Probability Measures*. Birkhäuser Verlag, Boston, 2008.
- [2] A. R. A. Anderson, M. A. J. Chaplain, and K. A. Rejniak, editors. *Single-cell-based models in biology and medicine*. Birkhäuser, 2007.
- [3] N. Bellomo, B. Piccoli, and A. Tosin. Modeling crowd dynamics from a complex system viewpoint. *Math. Models Methods Appl. Sci.*, 22:1230004, 2014.
- [4] V. Capasso and D. Morale. Asymptotic behavior of a system of stochastic particles subject to nonlocal interactions. *Stoch. Anal. Appl.*, 27:574–603, 2009.
- [5] V. Capasso and D. Morale. Stochastic modelling of tumour-induced angiogenesis. *J. Math. Biol.*, 58:219–233, 2009.
- [6] J. A. Carrillo, M. Fornasier, G. Toscani, and F. Vecil. Particle, kinetic, and hydrodynamic models of swarming. In G. Naldi, L. Pareschi, and G. Toscani, editors, *Mathematical Modeling of Collective Behavior in Socio-Economic and Life Sciences*, Modeling and Simulation in Science, Engineering and Technology, pages 297–336. Birkhäuser, Boston, 2010.
- [7] A. Colombi, M. Scianna, and L. Preziosi. A measure-theoretic model for cell migration and aggregation. Submitted.
- [8] E. Cristiani, B. Piccoli, and A. Tosin. Multiscale modeling of granular flows with application to crowd dynamics. *Multiscale Model. Simul.*, 9:155–182, 2011.
- [9] E. Cristiani, B. Piccoli, and A. Tosin. *Multiscale Modeling of Pedestrian Dynamics*. Springer, 2014 (In press).
- [10] V. Cristini and J. Lowengrub. *Multiscale modeling of cancer: an integrated experimental and mathematical modeling approach*. Cambridge University Press, 2011.
- [11] A. Deutsch and S. Dormann. *Cellular automaton modeling of biological pattern formation: characterization, applications, and analysis*. Birkhäuser, Boston, 2005.
- [12] M. Di Francesco and S. Fagioli. Measure solutions for non-local interaction pdes with two species. *Nonlinearity*, 26:2777, 2013.
- [13] D. Drasdo. Coarse graining in simulated cell populations. *Adv. Complex Syst.*, 8:319–363, 2005.
- [14] D. Drasdo. On selected individual-based approaches to the dynamics of multicellular systems. In *Multiscale Modeling*, pages 169–203. Birkhäuser Verlag, Boston, 2005.
- [15] P. Friedl and D. Gilmour. Collective cell migration in morphogenesis, regeneration and cancer. *Nat. Rev. Mol. Cell. Biol.*, 10:445–457, 2009.
- [16] O. Ilina and P. Friedl. Mechanisms of collective cell migration at a glance. *J. Cell Sci.*, 122:3203–3208, 2009.
- [17] D. Morale, V. Capasso, and K. Oelschläger. An interacting particle system modelling aggregation behavior: from individuals to populations. *J. Math. Biol.*, 50:49–66, 2005.
- [18] B. Piccoli and F. Rossi. Transport equation with nonlocal velocity in Wasserstein spaces: convergence of numerical schemes. *Acta Appl. Math.*, 124:73–105, 2013.
- [19] B. Piccoli and F. Rossi. Generalized Wasserstein distance and its application to transport equations with source. *Arch. Rational Mech. Anal.*, 211:335–358, 2014.

- [20] B. Piccoli and A. Tosin. Pedestrian flows in bounded domains with obstacles. *Contin. Mech. Thermodyn.*, 21:85–107, 2009.
- [21] B. Piccoli and A. Tosin. Time-evolving measures and macroscopic modeling of pedestrian flow. *Arch. Ration. Mech. Anal.*, 199:707–738, 2011.
- [22] M. Scianna and L. Preziosi. Multiscale developments of the cellular Potts model. *Multiscale Model. Simul.*, 10:342–382, 2012.
- [23] M. Scianna and L. Preziosi. *Cellular Potts Models: Multiscale Developments and Biological Applications*. Chapman & Hall/CRC Press, 2013.
- [24] A. Stevens. The derivation of chemotaxis equations as limit dynamics of moderately interacting stochastic many-particle systems. *SIAM J. Appl. Math.*, 61:183–212, 2000.
- [25] A. Tosin and P. Frasca. Existence and approximation of probability measure solutions to models of collective behaviors. *Netw. Heterog. Media*, 6:561–596, 2011.